DOI: 10.1021/ma9021696

Macromolecules
ARTICLE

Thermal Response of Surface Grafted Two-Dimensional Polystyrene (PS)/Polyvinylmethylether (PVME) Blend Films

Sebastian Lenz,[†] Sebastian K. Nett,[†] Mine Memesa,[†] Robert F. Roskamp,[†] Andreas Timmann,[‡] Stephan V. Roth,[‡] Rüdiger Berger,[†] and Jochen S. Gutmann*[,†,§]

[†]*Max Planck Institute for Polymer Research, Ackermannweg 10, D-55128 Mainz, Germany,* [‡]*HASYLAB at DESY, Notkestr. 85, D-22603 Hamburg, Germany, and* [§]*Institute for Physical Chemistry, Johannes Gutenberg University, Jakob-Welder-Weg 10, D-55099 Mainz, Germany*

Received September 30, 2009; Revised Manuscript Received December 4, 2009

ABSTRACT: This work shows that phase separations in 2D polymer films can be tuned by employing entropically constraining grafting points. We present experimental results on surface-grafted 2D polystyrene (PS)/polyvinylmethylether (PVME) blended films using surface-anchored benzophenone derivates. In contrast with 2D films that have not been grafted, it was possible to raise the blended lower critical solution temperature (LCST) above room temperature by using low grafting point densities. Highly constrained films did not show polymer−polymer phase separation. In addition to the in situ structural analysis performed with surface probe microscopy (SPM), μ-beam-sized grazing incidence small-angle X-ray scattering (μ-GISAXS), and μ-X-ray reflectivity (μ-XRR), surface stress investigations performed using nanomechanical cantilever sensor (NCS) arrays gave detailed insight into the phase separation mechanism. Phase separations were shown to result in dominating attractive entropic spring mechanisms with opposing repulsive effects resulting from surface and interfacial energy changes.

Introduction

Switchable polymer systems are of high interest for the application of thin films, which exhibit changes in surface properties under the influence of external stimuli.[1] Thermoresponsive polymer blend films undergo phase transitions at elevated temperatures, causing changes in surface properties. The polystyrene (PS)/polyvinylmethylether (PVME) film blend is one such an example, where this polymer mixes macroscopically at room temperature (RT) but shows a demixed two-phase state at high temperatures.[2−5] For a dip-coated 2D PS/PVME film, Tanaka et al.[6] proposed that the PVME phase dewets from the PS phase, allowing the PVME's conformational entropy loss to be recovered below RT.

Our aim was to raise the lower critical solution temperature (LCST) above RT (Figure 1). It was therefore necessary to constrain the ability of the PVME to recover its conformational entropy. This was achieved by introducing chain/surface grafting points by grafting the desired polymer blend to UV-sensitive linking layers. Prefunctionalized UV-sensitive surfaces were prepared using benzophenone end-functionalized silanes.[7] The use of such unspecific silane linkers resulted in surface-grafted polymer chains, which were immobilized by more than one chain segment to the substrate's surface.

Varying the density of active UV-sensitive groups allowed the grafting point density to be controlled and the ability of the chains to recover their conformational entropy losses accordingly. Consequently, the blended LCST could be controlled by different preparation routes of the silane grafting layers.

Phase transitions in thin films are related to the interfacial energy and volume changes, which induce surface stresses to the substrate. These usually small surface stress changes could be resolved using thick nanomechanical cantilever sensors (NCSs) as a sensor platform.[8−12] The arrangement of NCS in arrays and the possibility of coating individual NCS sensors with the desired coating allowed the use of internal cantilevers as a reference.[13] Therefore, it was possible to retrieve the corrected stress data resulting from various polymer coatings. In this manner, the stress changes in the polymer coatings during thermal treatments,[10−12] polymer brush swelling,[14−16] and polyelectrolyte adsorption[17] could be studied. In contrast with the commonly used deflection-based NCS read-out techniques,[9] an imaging interferometer[18] was used to measure the topography of the whole sensor array. As a result, a direct relation between the NCS curvatures and the absolute surface stresses was possible.

The measured surface stresses were also related to the structural changes, such as the formation of dewetted polymer domains. For better comparability, μ-beam-sized grazing incidence small-angle X-ray scattering (μ-GISAXS), and μ-beam sized X-ray reflectivity (μ-XRR) were performed on similarly prepared NCS sensor arrays.[19,20]

Materials and Methods

Nanomechanical Cantilever Arrays. NCS arrays (Octosensis, Micromotive Mikrotechnik, Germany) were used as flexible mechanical transducer elements and substrates for μ-GISAXS and μ-XRR experiments. Each array consisted of eight individual rectangular cantilevers having an area of $500 \times 90\ \mu m^2$, a thickness of 2 μm, a pitch of 250 μm, elastic modulus of $E = 130$ GPa and Poisson ratio $\nu = 0.28$.

Silane Solutions. 4-(3′-Triethoxysilyl)propoxybenzophenone (EtOH-silane) was prepared, as described elsewhere.[21] EtOH-silane films were prepared from a solution of EtOH-silane in ethanol (c = 2 mmol/L). 4-(3′-Chlorodimethylsilyl)propyloxybenzophenone (Cl-silane) was synthesized according to the method reported in the literature.[7] It is well-known that the benzophenone carbonyl unit can be deactivated by the presence of Pt catalysts.[7,22] This allows carbonyl reductions. However, to

*Corresponding author. E-mail: gutmann@mpip-mainz.mpg.de.

 Published on Web 12/30/2009

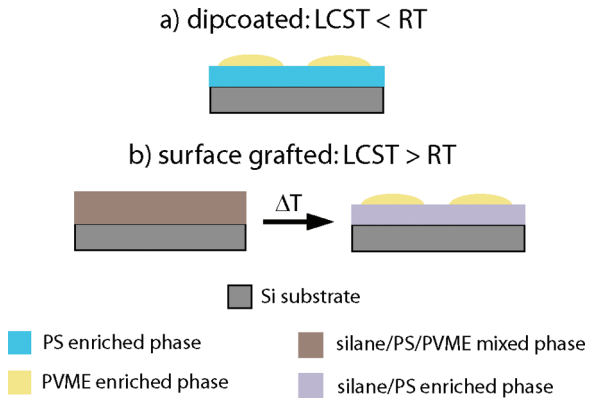

Figure 1. (a) Phase-separated 2D PS/PVME film prepared by dip coating.[6] (b) Expected dewetting mechanism at T > RT of a constrained, surface-anchored PS/PVME film.

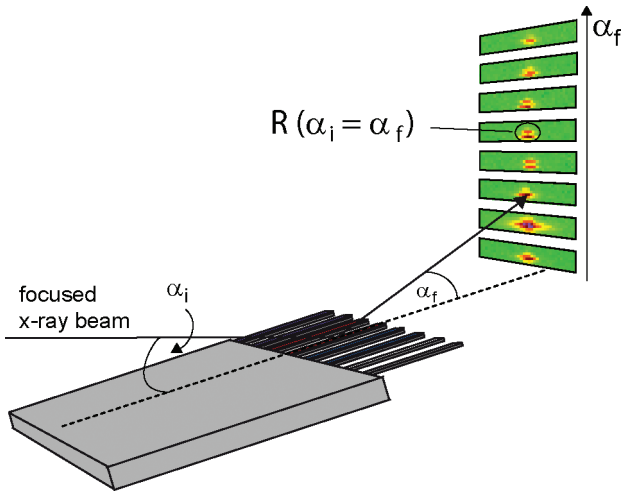

Figure 2. Geometry of a μ-XRR scan.

obtain only partially active benzophenone surfaces, the Pt−C catalyst was not removed from the product. We prepared fresh 0.024 mol/L Cl-silane solution by consecutively adding 0.4 mL of freshly distilled triethyl-amine and 0.2 mL of Cl-silane to 25 mL of dry toluene.

Grafted Polymers. Polystyrene (PS) was prepared by an anionic polymerization technique. The PVME that was used was purchased from Polysciences (Niles, IL). Molecular weights and weight distributions of the polymers were assigned using gel permeation chromatography (GPC). In the case of the PS, the M_n was found to be 26 700 g/mol with a polydispersity index (PDI) of 1.05. The average M_n of PVME was 66 000 g/mol, and the PDI was 8. PS/PVME blended films were prepared from a 1 wt % solution of toluene using a ratio of PS/PVME = 0.2 wt %.

Preparation of Grafted to Polymer Films on Flexible NCS Arrays. The NCS arrays for the differential bending, μ-GISAXS, and μ-XRR experiments were first dipped into a NH_3/H_2O_2 mixture in Millipore water at 80 °C for 20 min to obtain a controlled hydration of the native SiO_x surface. To obtain the NCS bending data, which can be related to surface stresses in the functional films, it was crucial to coat selectively the top of the NCS. Selective coating was achieved by passivating the backsides of the NCS arrays with a gold layer via thermal evaporation (20 nm, 0.1 nm/s, $p \approx 1.8 \times 10^{-5}$ mbar) (BALTEC MED 020, BALTEC, Balzers, Lichtenstein). The UV-sensitive linking layer was subsequently applied to the unprotected NCS topside by immersion of the arrays into a stirred linker solution under an argon atmosphere. The silane solutions, prepared in the manner described above, were then allowed to react for 48 h in the case of EtOH-silane functionalizations and for ca. 15 h in the case of Cl-silane functionalizations. The NCS arrays were cleaned by Soxhlet extraction in CH_2Cl_2 for 3 h after silanization. To allow differential bending experiments to be performed, individual signals from the polymer-grafted NCS and the reference NCS, such as the NCS functionalized only with the silanes, needed to be recorded simultaneously. Therefore, polymer blended and homopolymer solutions were selectively applied to single NCS using a video-assisted spot deposition technique.[23,24] Solution droplets were drop cast with a piezo-controlled nanoliter pipet using a Nano-Plotter NP2.0 device (GeSim, Germany). After drying in air, the dispensed polymer blend was grafted to the UV-sensitive benzophenone group under UV irradiation at λ = 365 nm for 1 h. Unbound polymer was extracted from the arrays with a Soxhlet extraction using CH_2Cl_2 for ca. 12 h. Using this sample preparation protocol, it was ensured that the reference NCS and the polymer-grafted NCS from the same array were treated equally. As a result, bending experiments, in combination with μ-GISAXS and μ-XRR studies were possible.

Preparation of Grafted to Polymer Films on Si Wafers. The preparation of silane layers on the Si-wafers was the same as that used for the NCS arrays, with the exception of the passivating gold layer. The polymer solutions were drop cast on the prefunctionalized substrates. After drying in vacuum, crosslinking and removal of excess polymer was performed in the manner explained above.

Scanning Probe Microscopy Studies. Scanning probe microscopy (SPM) images of EtOH-silane and Cl-silane blend grafted films were recorded in tapping mode at RT and at 150 °C in a defined environment of N_2 gas (environmental SPM, Veeco Instruments, Santa Barbara, CA). For these studies, silicon cantilevers were used, which had a nominal spring constant of 42 N/m and a resonance frequency of ~300 kHz (Olympus, OMCL-AC160TS, Japan). We used a NanoScope IIIa controller (Veeco Instruments, Santa Barbara, CA) controlled by the software 5.30r2 to operate the SPM. We removed the offset and tilt background of all images by processing all images with a first-order flattening procedure.

X-ray Reflectivity on Si-Wafers. X-ray reflectivity (XRR) experiments on the prepared EtOH-silane prefunctionalized Si wafers were performed on a $\theta-\theta$ XRD 3003 (Seifert Ltd., GB) diffractometer. Monochromatic and collimated Cu-Ka (l = 1.54 Å) X-rays were supplied by a Cu anode. For heating experiments, a custom-made oven was applied to the experimental setup, and measurements were performed at RT and 150 °C under a constant flow of N_2 until $2\theta_{max} = 6°$.

***μ*-GISAXS/*μ*- X-ray Reflectivity on NCS Arrays.** The μ-GISAXS and μ-XRR studies on Cl-silane NCS arrays were conducted at beamline BW4, HASYLAB at DESY, working at a wavelength of λ = 0.138 nm. Both μ-GISAXS and μ-XRR studies were performed at RT and 150 °C at the same Cl-silane NCS array, which was partially grafted with the PS/PVME blend and the homopolymers described above. The NCS array was mounted into a custom-made environmental sample cell. The capton sealed cell was purged with N_2 and heated to T = 150 °C. As a result, studies on the structural changes in the functional films upon phase transitions became accessible. The sample cell was mounted onto a two circle goniometer equipped at an x/y/z translation stage positioned in a sample to detector distance of ~2.1 m. To be able to address a single NCS with the illuminating X-ray beam, we used the microfocus option available at BW4.[19,20] The Gaussian fwhm beam dimension focused on the NCS was of a size of 32 × 17 μm^2 (horizontal × vertical). The μ-sized beam allowed the X-ray illumination of one single NCS. Static measurements at a constant incident angle of α_i = 0.74° were performed to obtain typical GISAXS patterns (Figure 3). During the reflectivity scans, the NCS was illuminated for a short time at $0.1 \leq \alpha_i \leq 1.8°$ at various steps (Figure 2). As a result, the beam's specular intensity versus

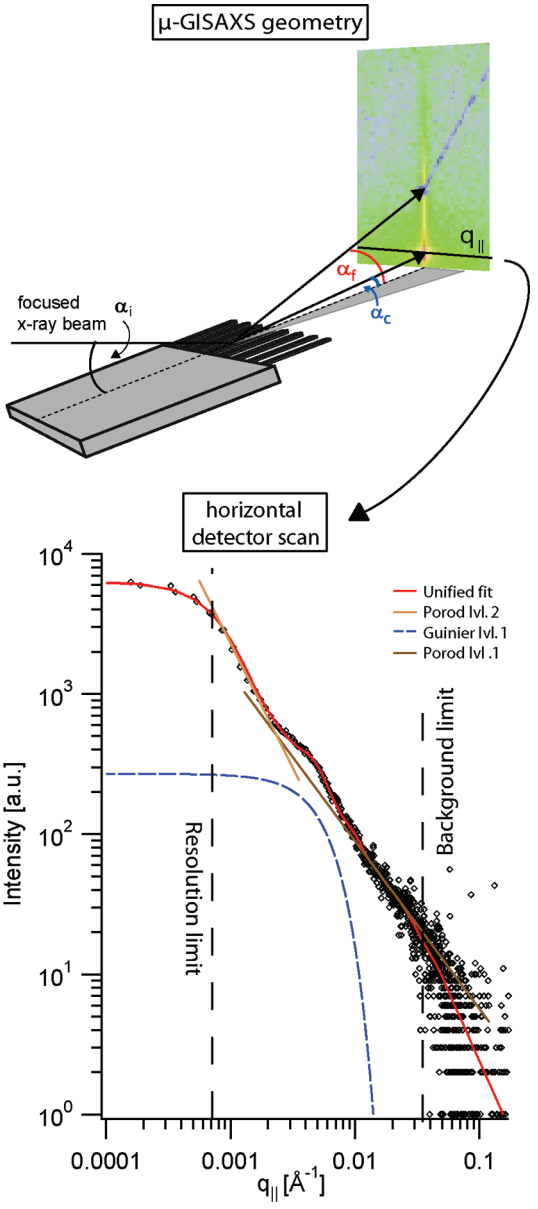

Figure 3. μ-GISAXS geometry (upper scheme); horizontal detector scans (lower graph) along the $q_{||}$ scattering plane were extracted from 2D scattering patterns at the maximum at the Yoneda peak's maximum. GISAXS data in the range of $0.007 < q_{||} < 0.025$ Å^{-1} were analyzed with the unified fit approach.

α_i was recorded and transformed into reflectivity curves, which were then analyzed with the Parratt's formalism.[25,26]

***μ*-GISAXS Analysis.** We obtained the lateral polymer domain size and distance estimations of the dewetted polymer films by performing horizontal detector scans along the reciprocal $q_{||}$ scattering plane (Figure 3). Under experimental conditions, the GISAXS resolution was limited by the reflected beam for $q_{||} < 0.007$ Å^{-1} and by background scattering for $q_{||} > 0.025$ Å^{-1}. Therefore, the GISAXS analysis was performed in a $q_{||}$ range of $0.007 < q_{||} < 0.025$ Å^{-1}. This $q_{||}$ range corresponds to an interval of $5 < R_{g,||} < 190$ nm in real space.

GISAXS data were analyzed with a unified fit approach using the IRENA2 software package for IGOR Pro.[27] The unified approach was originally developed for the transmission SAXS analysis of nanoparticle and polymer samples.[28,29] The unified fit approach models scattering in terms of structural levels. It uses a combination of Porod and Guinier laws to define fractal dimensions and the radii of gyration, R_g.

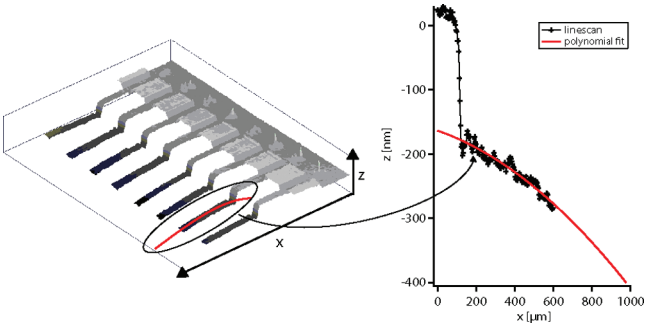

Figure 4. MCS array's 3D topography (left) with an extracted linescan (right). Curvatures were obtained from an approximation of the linescan based on second-order polynomials. The step of $\Delta z \approx 200$ nm accounts for the edge between supporting chip and NCS and denotes the x position of the NCS.

The scattered intensity can be written as a sum over i structural levels according to

$$I(q) \approx \sum_{i=1}^{n} G_i \exp\left(\frac{-q^2 R_{gi}^2}{3}\right) + B_i \exp\left(\frac{-q^2 R_{g(i-1)}^2}{3}\right)\left[\frac{(\mathrm{erf}(qR_{gi}/\sqrt{6}))^3}{q}\right]^{P_i} \quad (1)$$

where B and G are the Porod and Guinier prefactors, respectively, and P is the Porod exponent. A general structure factor ($S(q)$) is used to describe the domain correlations, which describes low correlated systems in terms of a packing factor, κ, and a mean correlation distance, ζ[27,30]

$$S(q) = \frac{1}{1 + 3\kappa(\sin(q\zeta) - q\zeta\cos(q\zeta))/(q\zeta)^3} \quad (2)$$

Simulations on GISAXS using the IsGISAXS software package[31] were used to estimate the maximum errors made using the unified fit model. Simulations from idealized structures at the film/air interface showed that errors resulting from the use of the transmission SAXS model for GISAXS analysis are $< 10\%$ for $R_{g,||}$ and $\zeta_{||}$.

NCS Bending Experiments. A custom-made interferometer was used to determine the NCS bending.[18] A laser having a wavelength of $\lambda = 780$ nm was used as the light source. The use of a CCD camera equipped to the interferometer device resulted in an imaging area of 1.28×0.96 mm^2. This allowed all eight NCS and parts of the supporting chip to be measured simultaneously. The NCS arrays were mounted to a custom-made environmental cell. The determination of the NCS bending was achieved via interferometric analysis, which was performed at RT and 150 °C under N_2 gaseous atmosphere. This temperature is close to the bulk demixing temperature that was determined by DSC (Supporting Information). OPTOCAT software (Breuckmann GmbH, Germany) was used to record the 3D topographies of the NCS arrays (Figure 4) at RT and 150 °C. Long time experiments over 24 h at 150 °C were performed, taking one topography image every 10 min.

To obtain surface stress related curvature data, topography profiles along the NCS x axes were performed. The resulting length/height data were modeled with a parabolic height profile[32] according to

$$z(x) = a_0 + a_1 x + \frac{\kappa}{2} x^2 \quad (3)$$

In eq 3, $z(x)$ denotes the deflection of the NCS at each position x along the NCS. Assuming that NCS is bent uniformly, the

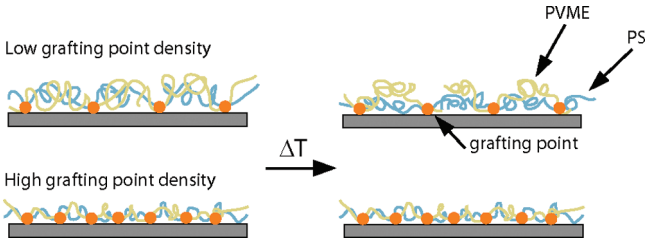

Figure 5. Schematic representation of the thermo response of surface anchored 2D PS/PVME blend in the case of low and high grafting point densities; low grafted blend films showed dewetting of the PVME from the mixed silane/PS phase; in highly grafted/entropically constrained films, dewetting is suppressed.

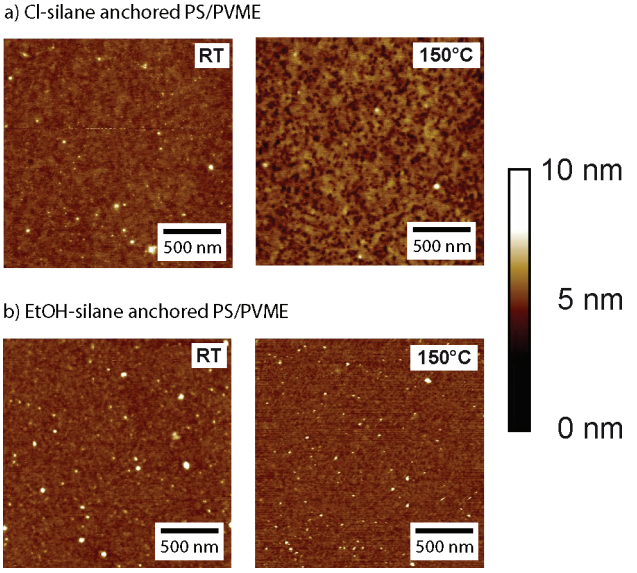

Figure 6. SPM height images at RT and 150 °C of PS/PVME films grafted to (a) Cl-silane prefunctionalized surface and (b) EtOH-silane prefunctionalized surface.

change of curvature $\Delta\kappa = \kappa_2 - \kappa_1$ can be calculated using $\kappa = d^2z(x)/(dx^2)$. To improve the statistics, curvatures of equally coated NCS were averaged.

Results and Discussion

It is well known that the properties of polymer brush systems are highly dependent on their grafting densities.[33,34] In contrast with, for example, end-grafted polymer brush films, polymer chains that are grafted to benzophenone functionalized surfaces are grafted unspecifically at more than one chain segment to the surface (Figure 5). Varying the grafting densities of the benzophenone functionalized silanes alters the number of polymer/surface grafting points per chain and introduces entropic constraints to the demixing polymer blend films. For grafted polymer blend systems showing LCST behavior, such as the PS/PVME blend, entropic constraints should lead to an increase in the LCST. This is because the PVME dewets under recovering the conformational entropy in the 2D film.[6] Therefore, increasing the number of entropic constraints should raise the LCST to higher temperatures.

SPM Results. As a first proof of the latter discussion, in situ SPM studies were performed to demonstrate that the densely grafted Cl-silane/PS/PVME films have an LCST of RT < T_{LCST} < 150 °C, whereas highly grafted EtOH-silane/PS/PVME did not show a phase separation effect (Figure 6). SPM height images of the Cl-silane/PS/PVME recorded at RT and at 150 °C (Figure 6a) under an inert gas atmosphere

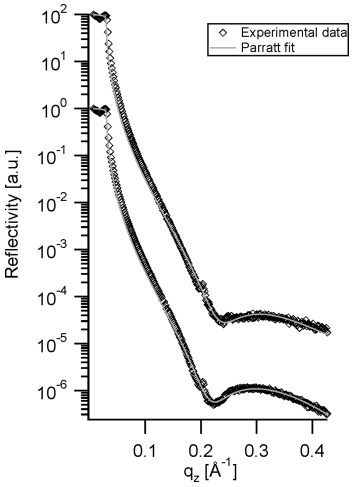

Figure 7. XRR curves of the non phase separating EtOH-silane/PS/PVME blend at RT (lower graph) and 150 °C (upper graph); reflectivity curve for the heat-treated sample is shifted by a factor of 100.

from the same specimen showed an increase in RMS roughness from 0.3 ± 0.1 to 0.6 ± 0.1 nm. In contrast, EtOH-silane/PS/PVME films showed no changes in RMS roughness at 150 °C (Figure 6b).

The roughness increase during annealing was attributed to the formation of polydisperse domains with average diameters of 60 ± 15 nm. The domains did not show a long-range order, but the average center-to-center distances were 110 ± 25 nm, and the average domain heights were 2 ± 1 nm. Dewetting of the PVME from the miscible Cl-silane/PS phase is assumed according to dewetting mechanisms in nonanchored films.[6] As a result, we could conclude that the benzophenone deactivation approach we used was suitable to reduce the number of benzophenone grafting points. From the domain height estimations of ~2 nm and based on the work of Shuto et al.,[35] one can estimate that the vertical chains, $R_{g,\perp}$, would be a factor of ~9 lower than the R_g of an unperturbated PVME chain. This implies that the chains were still in a constrained conformation state after phase separation.

X-ray Reflectivity Results. XRR studies performed on EtOH-silane grafted PS/PVME films revealed a film thickness of 1.5 ± 0.1 nm (Figure 7). The film thickness did not change during heat treatment. PVME was not able to dewet from the EtOH-silane/PS phase because of the high degree of grafting. Therefore, no phase separation process is observed for densely grafted EtOH-silane films. This result is in agreement with SPM data.

For a better comparability with surface stress investigations, μ-XRR was performed on NCS arrays coated with a Cl-silane grafted PS/PVME blend and homopolymer films. In addition, the use of one NCS array sample that was grafted individually ensured equal grafting point densities and equal environmental conditions for all film systems studied.

Experimental μ-XRR data (Figure 8) were fitted using the parratt's formalism.[25,26] The parameters that were obtained showed that the Cl-silane and PS films were of the equal thickness of 4 nm (Table 1). The estimated stretched length of the Cl-silane molecule is <1 nm. Therefore, a type of silane multilayer structure was observed within the approach used. The fact that the film thicknesses were equal supports the assumption of a hydrophobic mixed Cl-silane/PS phase. In the case of grafted PVME and PS/PVME systems, better fits were obtained using a two-layer model. According to the

two-layer model, the availability of functional benzophenone groups is small enough to allow the formation of second and lower dense phases. Consequently, PVME chains

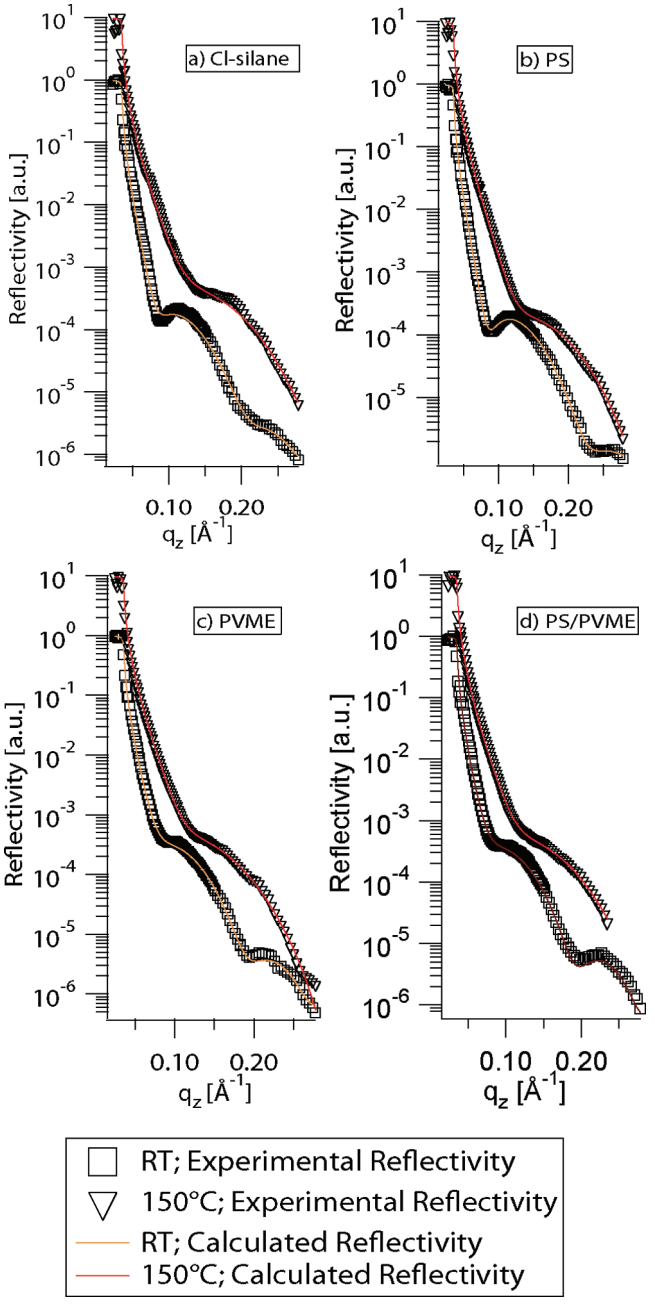

Figure 8. μ-XRR curves of (a) Cl-silane NCS, (b) Cl-silane/PS-grafted NCS, (c) Cl-silane/PVME-grafted NCS, and (d) Cl-silane/PS/PVME-grafted NCS at RT and 150 °C, respectively; reflectivity curves for heat-treated specimen are shifted by a factor of 10 for improved visualization.

do not seem to be completely miscible in the Cl-silane or in the miscible PS/Cl-silane phase. The Fresnel oscillations shifted to higher q_z values during the sample annealing. It was not possible to distinguish between a one- or two-layer system because of the absence of a second Fresnel minimum in the experimental q_z range. However, a decrease in the film thickness and a decrease in the material density could be obtained from the fits for all studied films. It therefore seems that the Cl-silane multilayer structure partially collapses with an accompanied decomposition during the heating process. Nevertheless, results from μ-GISAXS show that such Cl-silane film decompositions are not essentially disturbing the grafted polymers microstructure. The roughness values obtained for the Cl-silane and Cl-silane/PS films were found to be 0.3 nm at RT and did not change essentially during heating. For the Cl-silane/PVME films and the Cl-silane/PS/PVME films, the roughness at the film air interface was found to be ~0.2 nm, a value corresponding to the results obtained via SPM. As with the SPM results, heating was seen here to cause an increase in roughness to 0.7 nm in the Cl-silane/PS/PVME film, whereas the roughness of the Cl-silane/PVME film was seen to stay almost constant.

***μ*-GISAXS Results.** μ-GISAXS was performed on the same specimen and during the same heating period as μ-XRR. The use of μ-GISAXS allowed us to quantify more accurately the domain formations upon phase separation, which was observed by SPM. The elongation of the beam path under grazing incidence geometry allowed us to record the scattering averaged over the entire coated NCS (Figure 9).

According to the horizontal μ-GISAXS data of the Cl-silane and the Cl-silane/PS films, no interference peaks were observed at RT and 150 °C. Therefore, no lateral domain formation, which would form after dewetting, was observed. The outcome of this result is that the PS was seen to be miscible in the Cl-silane phase, as proposed from the μ-XRR experiments. The fact that dewetting effects were not seen for the Cl-silane lead to the conclusion that some of the Cl-silane material was lost in all of the polymer film systems during the heating process (thickness and density decrease shown in Table 1). However, the phase separation of the PS/PVME film is not essentially affected by this observation. The GISAXS data from the Cl-silane/PS/PVME film (Figure 9d) confirm that large structures of $R_{g,\parallel} = 28 \pm 2$ nm with average correlation distances of $\zeta_\parallel = 130 \pm 13$ nm form during heat treatment. These domains can be related to the polydisperse domains observed in the SPM images. Despite a partial Cl-silane degradation, such observation is again a clear indication of a dewetting process at RT < T_{LCST} < 150 °C. GISAXS from the Cl-silane/PVME film reveals an interference maximum at $q_\parallel \approx 0.002$ Å^{-1} at RT, which shifted to slightly higher $q_\parallel$ values during heat treatment (Figure 9c). From detailed analysis, $R_{g,\parallel}{}^{RT} = 30 \pm 3$ nm with $\zeta_\parallel{}^{RT} = 125 \pm 13$ nm and $R_g{}^{150°C} = 21 \pm 2$ nm with $\xi^{150°C} = 131 \pm 13$ nm could be assigned. In conjunction

Table 1. Fit Results of Film Thicknesses, *t*, Film Densities, *ρ*, and Roughness, *s*, from *μ*-XRR Curves (Figure 8)[a]

	Cl-silane		PS		PVME		PS/PVME	
	RT	150 °C	RT	150 °C	RT	150 °C	RT	150 °C
t^1 (nm)	4.1 ± 0.1	2.9 ± 0.2	4.0 ± 0.1	2.9 ± 0.2	3.4 ± 0.1	3.2 ± 0.2	3.4 ± 0.1	3.1 ± 0.2
ρ^1 (g·cm^{-3})	0.78 ± 0.01	0.45 ± 0.01	0.91 ± 0.01	0.47 ± 0.01	0.78 ± 0.02	0.50 ± 0.02	0.90 ± 0.02	0.46 ± 0.01
s^1 (nm)	0.31 ± 0.02	0.24 ± 0.1	0.33 ± 0.02	0.27 ± 0.1	0.43 ± 0.15	0.31 ± 0.05	0.58 ± 0.07	0.71 ± 0.03
t^2 (nm)					1.7 ± 0.1		1.5 ± 0.1	
ρ^2 (g·cm^{-3})					0.4 ± 0.1		0.4 ± 0.1	
s^2 (nm)					0.20 ± 0.10		0.15 ± 0.10	

[a] Superscripted index marks the number of the modeled layer starting from the Si Surface.

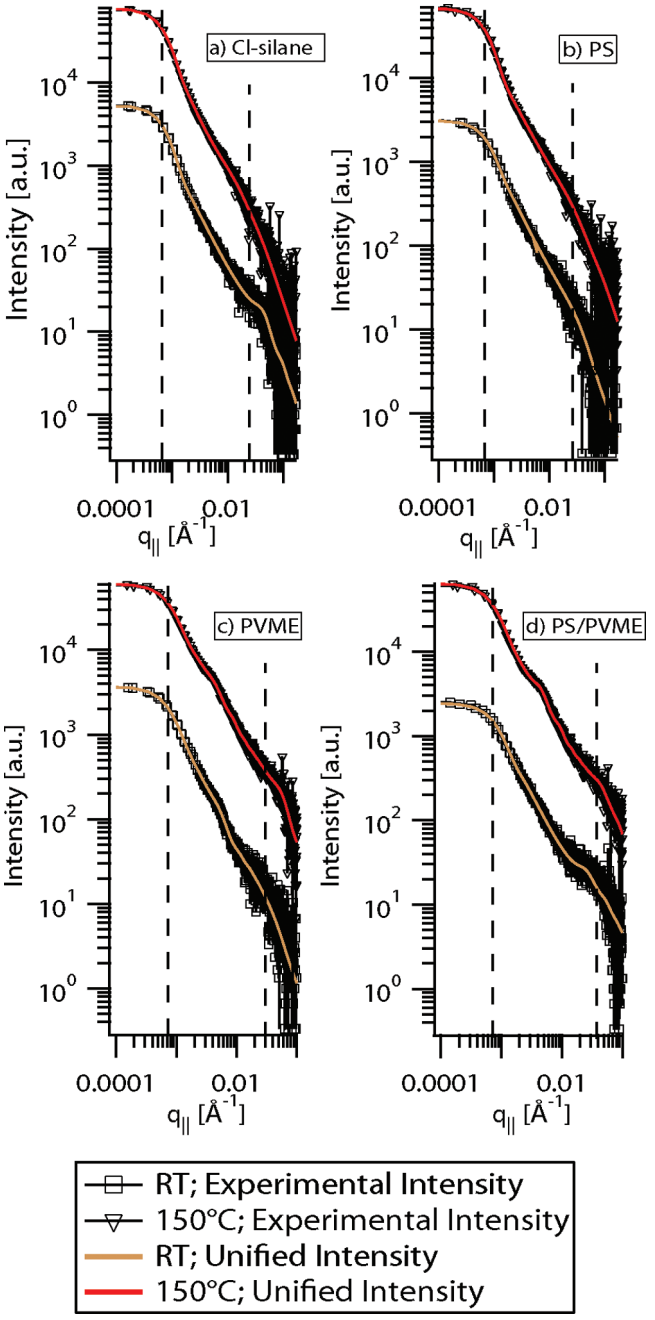

Figure 9. μ-GISAXS horizontal detector scans of Cl-silane NCS systems at RT and 150 °C. Black data points represent experimental data, brown and red lines represent the applied fit: (a) Cl-silane grafted NCS, (b) Cl-silane/PS grafted NCS, (c) Cl-silane/PVME grafted NCS, and (d) Cl-silane/PS/PVME grafted NCS. $q_{||}$ graphs for heat-treated specimen are shifted by a factor of 10 for improved visualization. Vertical dashed lines remark the resolution limits.

with the μ-XRR data, the μ-GISAXS experiments prove that PVME domains already dewet at RT from the hydrophobic Cl-silane surface. Annealing causes the PVME domains to shrink because of a contraction of the polymer chains at retaining correlation distances. As one can see, fitting parameters for the annealed Cl-silane/PVME and Cl-silane/PS/PVME films are similar. Therefore, PVME could be made to dewet from the Cl-silane by the addition of PS, and the LCST was raised above RT. This is because PS mixes without dewetting with the Cl-silane (Figure 9b). The addition of PS to the Cl-silane/PVME system suppresses the PVME dewetting at $T <$ RT. However, a PS/PVME enriched second layer of lower density was built as indicated by μ-XRR.

Surface Stress Results. In addition to the average structural information of the functional Cl-silane/PS/PVME films, interfacial energy and volume changes need to be considered to complete the physical picture of the phase separation mechanism. Interfacial energy and volume changes in the coated layer lead to attractive or repulsive forces, which are directed along the NCS. Transduced attractive forces lead to NCS bending toward the side of the coating with $\Delta\sigma > 0$ (corresponding to a tensile surface stress). Repulsive forces lead to a bending of the NCS away from the coating with $\Delta\sigma < 0$, corresponding to a compressive stress. Stoney's formula can be used to calculate the change in the surface stresses using thin film approximations

$$\Delta\sigma = \frac{E t_{\mathrm{NCS}}^2}{6(1-\nu)}\Delta\kappa \qquad (4)$$

where E is the substrate's Young's modulus, ν is the Poisson ratio, and t_{NCS} is the thickness of the NCS.

Polymer uncoated Cl-silane and EtOH-silane curvature data taken at 150 °C were baseline corrected for RT curvature values according to $\Delta\kappa(\mathrm{silane})^{150°\mathrm{C\text{-}RT}} = \kappa(\mathrm{silane})^{150°\mathrm{C}} - \kappa(\mathrm{silane})^{\mathrm{RT}}$. Polymer-coated NCS curvature data taken at 150 °C were corrected for pure silane curvatures and baseline corrected for RT curvature values according to $\Delta\kappa(\mathrm{polymer})^{150°\mathrm{C\text{-}RT}} = \Delta\kappa(\mathrm{silane/polymer})^{150°\mathrm{C}} - \Delta\kappa(\mathrm{silane/polymer})^{\mathrm{RT}} - \Delta\kappa(\mathrm{silane})^{150°\mathrm{C\text{-}RT}}$. From $\Delta\kappa^{150°\mathrm{C\text{-}RT}}$ data, $\Delta\sigma^{150°\mathrm{C\text{-}RT}}$ data was obtained according to eq 4. In such a way, conclusions could be made on the surface stress changes of the polymer coatings, corrected for effects from transitions in the silane layers.

No essential curvature and stress changes could be observed from the bending data obtained from the EtOH-silane and the EtOH-silane/PS/PVME films (triangles in Figure 10). Such behavior is expected, because SPM and XRR results clearly indicate that no phase transitions occurred in the highly entropic constrained EtOH-silane/PS/PVME systems.

In contrast, pronounced surface stress changes upon annealing were observed for polymer systems grafted to the low constraining Cl-silane functionalized surfaces (filled circles in Figure 10). For an ungrafted Cl-silane film, compressive surface stress changes of $\Delta\sigma = -0.22 \pm 0.05$ N/m were calculated. In contrast, Cl-silane coated NCS of equal thicknesses showed tensile stresses due to bimaterial effects in the order of $\Delta\sigma = 0.44 \pm 0.05$ N/m. Such observed compressive stresses were related to a partial collapse of the Cl-silane multilayer structure. The compressive surface stresses in Cl-silane layers, however, reversed to tensile when stresses from the PS, the PVME, and the PS/PVME coatings were studied. Such behavior cannot be attributed to a typical bimaterial effect, where the polymer film would isotropically expand and compressive stresses would be measured.

The total magnitudes of tensile stresses after correction for the Cl-silane reference that resulted from annealing were $\Delta\sigma^{150°\mathrm{C\text{-}RT}}$ (PS) $= 0.52 \pm 0.05$ N/m, $\Delta\sigma^{150°\mathrm{C\text{-}RT}}$ (PVME) $= 0.34 \pm 0.05$ N/m, and $\Delta\sigma^{150°\mathrm{C\text{-}RT}}$ (PS/PVME) $= 0.26 \pm 0.05$ N/m. The physical reason for the detected tensile stresses could be revealed by considering the fact that the μ-GISAXS results indicated a shrinking of the RT dewetted PVME domains during annealing. Polymer domain shrinking is accompanied by entropically driven chain contractions. PVME domains are only 1.7 ± 0.1 nm thick, as measured by μ-XRR. Such small domain thicknesses clearly indicate that the polymer chains are grafted at more than one

chain segment to the NCS substrate. The resulting attractive force can therefore be transferred to the NCS substrate. Consequently, tensile stresses are measured. As the NCS arrays are prepared in parallel, the grafting point densities were assumed identical for all polymer-films grafted to the same NCS array. Similar Cl-silane grafting point densities allow comparisons to be made between the different polymer systems. Consequently, attractive forces within the polymer films resulting from the discussed entropy changes can be assumed to be similar and irrespective of the molecular weight for all three grafted films according to

$$\Delta F_{\text{entrop.}}^{\text{Cl-silane/PS}} \approx \Delta F_{\text{entrop.}}^{\text{Cl-silane/PVME}} \approx \Delta F_{\text{entrop.}}^{\text{Cl-silane/PS/PVME}} < 0 \quad (5)$$

As a result, similar tensile surface stress proportions are expected by only regarding entropic chain contractions. Nevertheless, the total magnitudes of tensile stresses are clearly dependent on the grafted polymer systems. Figure 11 gives an illustrative overview of the structural and the mechanical changes of all polymer grafted film systems.

Tensile stresses, which were corrected for the Cl-silane reference, resulting from annealing are $\Delta\sigma^{150°C\text{-}RT}$ (PS) = 0.52 ± 0.05 N/m, $\Delta\sigma^{150°C\text{-}RT}$ (PVME) = 0.34 ± 0.05 N/m and $\Delta\sigma^{150°C\text{-}RT}$ (PS/PVME) = 0.26 ± 0.05 N/m. (See Figure 11).

The annealing temperature of 150 °C is above the glass-transition temperature of the bulk PS of ~100 °C. Jung et al.[12] have measured a decrease in compressive stresses for expanding PS films because of a softening of the material for $T > T_g$. Transferring their result to our contracting polymer films, the transition from a glassy to a soft rubbery film would lead to a decrease in tensile stress. However, measured tensile stresses of Cl-silane/PS films were higher than those of Cl-silane/PVME films, which have a bulk T_g of −40 °C. It may be doubted that the constrained polymer films undergo glass transitions in the studied temperature range. Such dramatic change in T_g would be consistent with T_g changes

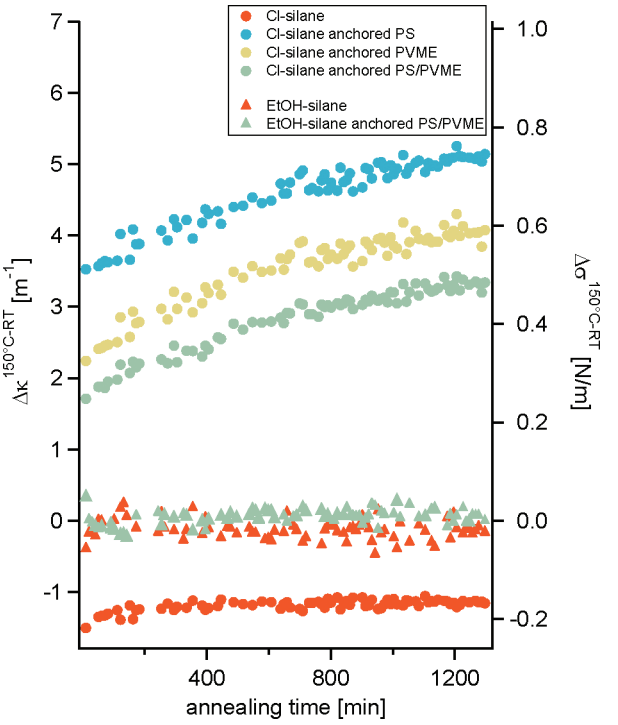

Figure 10. Curvature and stress changes versus time data extracted from interferometric measurements of Cl-silane and EtOH-silane systems. All curves were baseline-corrected for RT values. Curvature and stress data from polymer-grafted systems were corrected for reference Cl-silane data. Errors resulting from curvature analysis are corresponding to the size of data points. Scattering of data points is related to the intrinsic maximum error of ±0.05 N/m of the used technique.

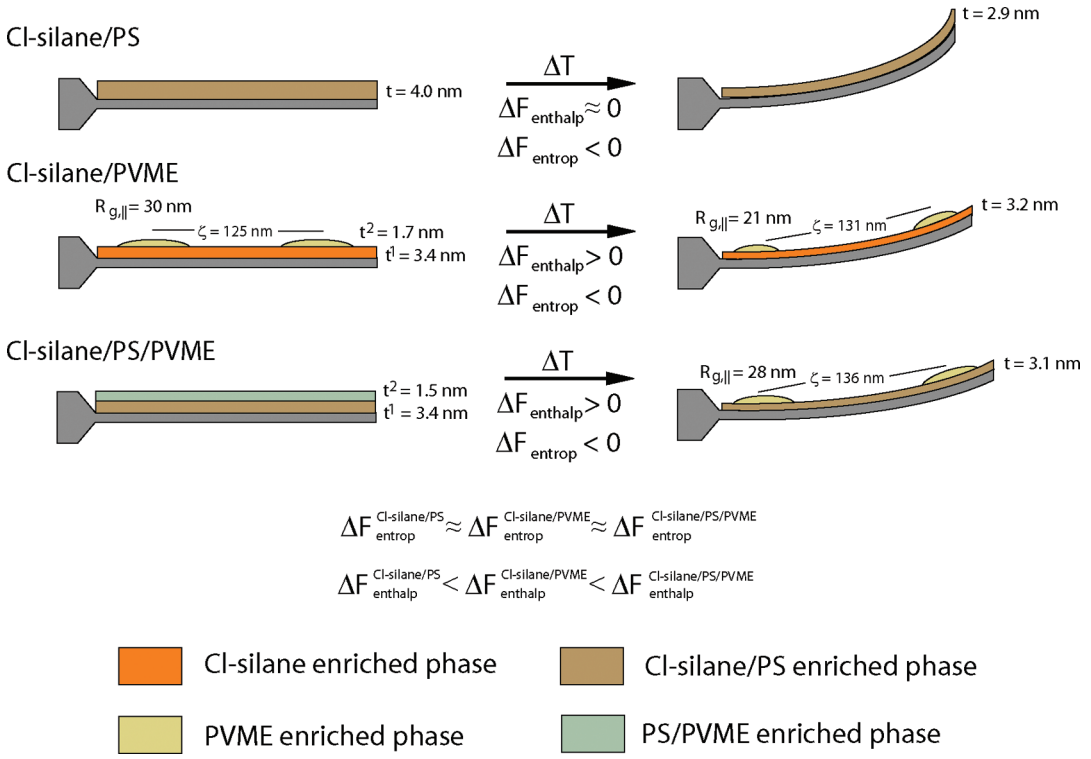

Figure 11. Illustrative scheme of the proposed mechanisms resulting from annealing the grafted polymer systems. In the presented scheme, main results obtained from μ-GISAXS and μ-XRR are related to proposed entropic driven attractions and interfacial repulsions.

in ultrathin polymer films resulting from wall confinements[36] and cross-linked polymer systems.[37] However, these assumptions have to be studied in detail by comparative experimental studies.

Apart from glass transitions, superimposed repulsive forces that result from the surface and interfacial energies cannot be neglected. For such argumentation, the magnitudes and directions of the forces resulting from surface energy and interfacial energy changes need to be discussed.

First, the surface energy of the film/air interface can change upon annealing. Such energy changes can be attributed to changes in the surface tensions of the grafted polymers. Bulk PS and PVME have similar surface tensions of $\gamma(\mathrm{PS})^{\mathrm{RT}} = 40.2\ \mathrm{mJ/m^2}$ and $\gamma(\mathrm{PVME})^{\mathrm{RT}} = 36.0\ \mathrm{mJ/m^2}$ at RT.[6] Both bulk polymers experimental and theoretical approaches[38,39] predict a nearly linear decrease in surface tensions with temperature according to $\mathrm{d}\gamma(\mathrm{PS})/\mathrm{d}t = 0.072$ and $\mathrm{d}\gamma(\mathrm{PVME})/\mathrm{d}t = 0.075$.[40] Such decreases in surface tensions lead to a decrease in the Gibbs surface energy, according to the relationship $\Delta G_{\mathrm{surface}}^{150°\mathrm{C}-\mathrm{RT}} \approx -A\Delta\gamma^{150°\mathrm{C}-\mathrm{RT}}$. Because the surface stress can be directly related to the Gibbs surface energy,[8] reductions in the Gibbs surface energies in the grafted films lead to compressive stresses of similar magnitude for all three polymer systems. Obviously the different magnitudes in the surface stress reductions cannot be explained exclusively by reductions in surface energies.

Therefore, the forces resulting from interfacial energy changes have to be regarded to explain the variation in the tensile stresses detected for the grafted homo and blended polymer films. The only interfacial contribution that was not similar for all systems and that is still reflected in differential $\Delta\kappa^{150°\mathrm{C\text{-}RT}}$ and $\Delta\sigma^{150°\mathrm{C\text{-}RT}}$ data can result from the Cl-silane/polymer interface.

According to the μ-GISAXS and μ-XRR results, it follows that the Cl-silane/PS film was in a microscopically mixed state at RT and did not phase separate during annealing. Therefore, interaction energy changes can be assumed to be small. The Cl-silane/PVME film was already found in a dewetted two-phase state at RT, as indicated by the μ-GISAXS and μ-XRR results. Considering the attractive chain contractions, it can be argued that intermolecular PVME chain interactions are favored, whereas intramolecular Cl-silane/PVME interactions are disfavored. In other words, shrinking PVME domains repel the Cl-silane grafting layer, which results in a lateral pressure. In contrast with the Cl-silane/PS films, such interfacial repulsive forces led to an NCS bending away from the coating layer in the Cl-silane/PVME film. The Cl-silane/PS/PVME was found to be not entirely mixed at RT, as indicated by the found two-phase film (Table 1). However, a PVME domain formation was not observed at RT (μ-GISAXS and SPM). Annealing caused a pronounced PVME domain formation, causing domains of similar sizes and domain center to center distances similar than that measured for the Cl-silane/PVME film by μ-GISAXS. The lower surface stress change detected for the Cl-silane/PS/PVME film compared with the Cl-silane/PVME film can therefore be attributed to an increased repulsion between the PVME chains and the mixed Cl-silane/PS phase. Following, the repulsive interfacial forces of the three comparable grafted polymer film systems are of enthalpic nature and can be related according to

$$0 \approx \Delta F_{\mathrm{interface}}^{\mathrm{Cl-silane/PS}} < \Delta F_{\mathrm{interface}}^{\mathrm{Cl-silane/PVME}} < \Delta F_{\mathrm{interface}}^{\mathrm{Cl-silane/PS/PVME}} \quad (6)$$

During constant annealing, the tensile stresses in all of the polymer films increase by a further 0.2 ± 0.05 N/m. These changes are equal for all polymer anchored films. They are therefore not attributed to individual stress changes caused by interfacial interaction energy changes but to continuous structural and conformational rearrangements. In summary, it can be concluded that attractive entropic driven conformation changes dominate the repulsive surface energy effects and the individual repulsions driven by the interfacial interaction energy changes. Therefore, dominating tensile stresses were detected.

Summary

We showed that phase-transition processes in grafted 2D PS/PVME polymer films could be tuned by changing the density of the active benzophenone grafting points. Our results show that the hydrophobic benzophenone linking layers with low grafting point densities at the surface are necessary for the observation of PVME dewetting in the studied temperature range. In such a way, it was possible to raise the blended LCST above RT. Such a behavior was not reported for dip-coated 2D films, where the LCST was found to be below RT.[6] Apart from a raise in LCST, the experimental results propose a similar PVME dewetting mechanisms as that proposed for dip-coated films. Because of conformational constraints caused by chain grafting at more than one segment, PVME chains were not to be able to recover all of their conformational energy. In addition to the dewetting processes, a collapse of the formed linker multilayer structure was observed. However, such a film collapse did not disturb the observed phase separation process. Combining the structural investigations with the surface stress investigations extracted from the NCS bending experiments allowed the film structure results to be understood in terms of energetic changes in the polymer films upon phase transition. Detected tensile stresses were related to attractive entropic spring mechanisms during conformational recovering of constrained chains. It was further proposed that attractive entropic effects were lowered by opposing repulsive processes, driven by decreasing surface tensions and interfacial repulsions. However, attractive effects were seen to dominate the repulsive effects during phase transition.

Acknowledgment. This research was supported by the Max Planck Society (Institutsübergreifende Forschungsinitiative FRM II), and the DFG priority program 1181 (GU771/2, MU1487/5). We gratefully thank the HASYLAB for provision of beamtime, Martin Dommach, and Ralph Döhrmann for technical support at the beamline BW4, Gunnar Kircher for support with sample preparation, Uwe Rietzler for SPM support and Dr. Cathy McNamee for careful revision of our manuscript.

Supporting Information Available: Supplementary DSC thermograph of the PS/PVME bulk film is provided. This material is available free of charge via the Internet at http://pubs.acs.org.

References and Notes

(1) Luzinov, I.; Minko, S.; Tsukruk, V. V. *Prog. Polym. Sci.* **2004**, *29*, 635–698.
(2) Bank, M.; Leffingw, J; Thies, C. *Macromolecules* **1971**, *4*, 43–46.
(3) Kwei, T. K.; Nishi, T.; Roberts, R. F. *Macromolecules* **1974**, *7*, 667–674.
(4) Nishi, T.; Kwei, T. K. *Polymer* **1975**, *16*, 285–290.
(5) Nishi, T.; Wang, T. T.; Kwei, T. K. *Macromolecules* **1975**, *8*, 227–234.
(6) Tanaka, K.; Yoon, J. S.; Takahara, A.; Kajiyama, T. *Macromolecules* **1995**, *28*, 934–938.
(7) Prucker, O.; Naumann, C. A.; Ruhe, J.; Knoll, W.; Frank, C. W. *J. Am. Chem. Soc.* **1999**, *121*, 8766–8770.
(8) Butt, H.-J. *J. Colloid Interface Sci.* **1996**, *180*, 251–260.

(9) *Springer Handbook of Nanotechnology*, 2nd. ed.; Bhushan, B., Ed.; Springer: New York, 2007.
(10) Zhao, J.; Berger, R.; Gutmann, J. S. *Appl. Phys. Lett.* **2006**, *89*, 033110.
(11) Jung, N.; Jeon, S. *Macromolecules* **2008**, *41*, 9819–9822.
(12) Jung, N.; Seo, H.; Lee, D.; Ryu, C. Y.; Jeon, S. *Macromolecules* **2008**, *41*, 6873–6875.
(13) Lang, H. P.; Berger, R.; Andreoli, C.; Brugger, J.; Despont, M.; Vettiger, P.; Gerber, C.; Gimzewski, J. K.; Ramseyer, J. P.; Meyer, E.; Guntherodt, H. J. *Appl. Phys. Lett.* **1998**, *72*, 383–385.
(14) Zhou, F.; Shu, W. M.; Welland, M. E.; Huck, W. T. S. *J. Am. Chem. Soc.* **2006**, *128*, 5326–5327.
(15) Bumbu, G. G.; Wolkenhauer, M.; Kircher, G.; Gutmann, J. S.; Berger, R. *Langmuir* **2007**, *23*, 2203–2207.
(16) Bradley, C.; Jalili, N.; Nett, S. K.; Chu, L. Q.; Forch, R.; Gutmann, J. S.; Berger, R. *Macromol. Chem. Phys.* **2009**, *210*, 1339–1345.
(17) Toda, M.; Itakura, A. N.; Igarashi, S.; Buscher, K.; Gutmann, J. S.; Graf, K.; Berger, R. *Langmuir* **2008**, *24*, 3191–3198.
(18) Helm, M.; Servant, J. J.; Saurenbach, F.; Berger, R. *Appl. Phys. Lett.* **2005**, *87*, 064101.
(19) Roth, S. V.; Dohrmann, R.; Dommach, M.; Kuhlmann, M.; Kroger, I.; Gehrke, R.; Walter, H.; Schroer, C.; Lengeler, B.; Muller-Buschbaum, P. *Rev. Sci. Instrum.* **2006**, *77*, 085106.
(20) Wolkenhauer, M.; Bumbu, G.-G.; Cheng, Y.; Roth, S. V.; Gutmann, J. S. *Appl. Phys. Lett.* **2006**, *89*, 054101.
(21) Gianneli, M.; Roskamp, R. F.; Jonas, U.; Loppinet, B.; Fytas, G.; Knoll, W. *Soft Matter* **2008**, *4*, 1443–1447.
(22) Marciniec, B. *Comprehensive Handbook on Hydrosilation*; Pergamon Press: Oxford, 1992.
(23) Bietsch, A.; Hegner, M.; Lang, H. P.; Gerber, C. *Langmuir* **2004**, *20*, 5119–5122.
(24) Bietsch, A.; Zhang, J. Y.; Hegner, M.; Lang, H. P.; Gerber, C. *Nanotechnology* **2004**, *15*, 873–880.
(25) Parratt, L. G. *Phys. Rev.* **1954**, *95*, 359–369.
(26) Nevot, L.; Croce, P. *Rev. Phys. Appl.* **1980**, *15*, 761–779.
(27) Ilavsky, J.; Jemian, P. R. *J. Appl. Crystallogr.* **2009**, *42*, 347–353.
(28) Beaucage, G. *J. Appl. Crystallogr.* **1995**, *28*, 717–728.
(29) Beaucage, G. *J. Appl. Crystallogr.* **1996**, *29*, 134–146.
(30) Beaucage, G.; Ulibarri, T. A.; Black, E. P.; Schaefer, D. W. *Hybrid Org.-Inorg. Compos.* **1995**, *585*, 97–111.
(31) Lazzari, R. *J. Appl. Crystallogr.* **2002**, *35*, 406–421.
(32) Korsunsky, A. M.; Cherian, S.; Raiteri, R.; Berger, R. *Sens. Actuators, A* **2007**, *139*, 70–77.
(33) Alexander, S. *J. Phys.* **1977**, *38*, 983–987.
(34) de Gennes, P. G. *Macromolecules* **1980**, *13*, 1069–1075.
(35) Shuto, K.; Oishi, Y.; Kajiyama, T.; Han, C. C. *Macromolecules* **1993**, *26*, 6589–6594.
(36) Forrest, J. A.; Dalnoki-Veress, K. *Adv. Colloid Interface Sci.* **2001**, *94*, 167–196.
(37) Fox, T. G.; Loshaek, S. *J. Polym. Sci.* **1955**, *15*, 371–390.
(38) Dee, G. T.; Sauer, B. B. *Macromolecules* **1993**, *26*, 2771–2778.
(39) Choi, K.; Jo, W. H.; Hsu, S. L. *Macromolecules* **1998**, *31*, 1366–1372.
(40) Brandrup, J.; Immergut, E. H.; Grulke, E. A. *Polymer Handbook*; Wiley: New York, 1999.